Optical Engineering

OpticalEngineering.SPIEDigitalLibrary.org

Diffraction analysis for digital micromirror device scene projectors in the long-wave infrared

Qing Han
Jian Wang
Jianzhong Zhang
Qiang Sun

Qing Han, Jian Wang, Jianzhong Zhang, Qiang Sun, "Diffraction analysis for digital micromirror device scene projectors in the long-wave infrared," *Opt. Eng.* **55**(8), 085105 (2016), doi: 10.1117/1.OE.55.8.085105.

Downloaded From: https://www.spiedigitallibrary.org/journals/Optical-Engineering on 9/9/2017 Terms of Use: https://spiedigitallibrary.spie.org/ss/TermsOfUse.aspx

Diffraction analysis for digital micromirror device scene projectors in the long-wave infrared

Qing Han,[a,b,*] **Jian Wang,**[b] **Jianzhong Zhang,**[b] **and Qiang Sun**[b]
[a]University of Chinese Academy of Sciences, 19 Yuquan Road, Beijing 100049, China
[b]Changchun Institute of Optics, Fine Mechanics and Physics, Chinese Academy of Sciences, 77 Yingkou Road, Changchun 130033, China

Abstract. Diffraction effects play a significant role in scene projectors by digital micromirror devices (DMDs) in the long-wave infrared (IR) band (8 to 12 μm). The contrast provided by these projector systems can become noticeably worse because of the diffraction characteristics of the DMD. The actual diffraction characteristics of the DMD deviate significantly from the predictions of scalar diffraction theory in the long-wave IR. To address this issue, we built a vector diffraction-grating model of the DMD; the diffraction grating model is simulated with MATLAB. Furthermore, we analyze the effect of incident angle and polarization, which are the main factors that decrease the contrast of DMD-based scene projectors in the long-wave IR. Finally, an effective method to improve the contrast of the scene projector system is given, and the maximum contrast of the scene projector system is ∼0.7. © *2016 Society of Photo-Optical Instrumentation Engineers (SPIE)* [DOI: 10.1117/1.OE.55.8.085105]

Keywords: digital micromirror device; scene projector; incident angle; diffraction analysis.

Paper 160968 received Jun. 20, 2016; accepted for publication Aug. 8, 2016; published online Aug. 23, 2016.

1 Introduction

The infrared (IR) scene projector is a core part in IR scene simulation systems and provides IR target and background imaging in IR tracking systems. Research on IR scene simulation systems began in the 1970s, and a variety of IR scene projectors have been developed since then, including resistive arrays, laser diode arrays, IR liquid crystal light valves, and digital micromirror devices (DMDs).[1,2] The DMD was invented by Texas Instruments in 1981 and was quickly used for IR scene projection. Moreover, the DMD-based IR scene projector developed rapidly because of its low cost, ultrastability, and high-quality imaging.[2,3]

To date, DMD-based IR scene projectors have found numerous applications in the near-IR (0.76 to 1.6 μm) and mid-IR (3 to 5 μm) ranges.[3–8] However, DMD-based scene projection in the long-wave IR (8 to 12 μm) is hampered by the diffraction characteristics of the DMD, which result in poor image contrast and concomitant poor imaging. To improve the contrast of DMD-based scene projectors, the diffraction characteristics of the DMD must be analyzed. In general, scalar diffraction theory is used to analyze the diffraction characteristics of the DMD.[9,10] However, in the long-wave IR, the experimental results deviate significantly from that predicted with scalar diffraction theory. The reason for this discrepancy is that the polarization of the incident beam comes into play when the incident wavelength is comparable to the size of the micromirror. Thus, a precise analysis requires the application of vector diffraction theory to describe the diffraction characteristics of the DMD in the long-wave IR.

We first use rigorous coupled-wave theory to characterize the diffraction of the DMD. In accordance with the structure and operating principle of the DMD, the DMD is treated as a metallic blazed diffraction grating. In addition, a detailed diffraction model of the DMD is presented to analyze the diffraction of the DMD; the simulation calculation is conducted with MATLAB. DMD diffraction efficiencies in the long-wave IR are presented with the incident angles of 20 to 60 deg and with transverse electric (TE) and transverse magnetic (TM) polarized. The simulation results indicate that the contrast of DMD-based scene projectors in the long-wave IR is ∼0.7 with an incident angle of 44 and 47 deg and with TM polarized. The diffraction grating model proposed in this study provides a method to improve the contrast of DMD-based scene projectors in the long-wave IR.

2 Diffraction Theory Applied to the DMD

2.1 *Operating Principle of the DMD*

The DMD consists of an array of aluminum micromirrors that can be rotated by electrostatic forces. It is used as a reflected spatial light modulator in DMD-based IR scene projectors. DMD operation is depicted in Fig. 1. Each DMD micromirror is used as a photoelectric switch with two working states: the on state and the off state. In the working states, each micromirror rotates either $+12$ deg (on state) or -12 deg (off state) from the flat state. When micromirrors rotate to $+12$ deg (-12 deg), the reflected light is steered into (out of) the projection aperture. Thus, the DMD is used as reflection spatial modulator, and images are produced with gray-scale modulation by rotating the micromirrors to the on (off) state.[2,3,12]

2.2 *Diffraction Model of the Digital Micromirror Devices*

According to the structure and operating principle, DMD is treated as a metallic blazed diffraction grating. Figure 2 shows the equivalent grating of the DMD, where the micromirror rotated angle θ is analogous to the grating blaze angle.

*Address all correspondence to: Qing Han, E-mail: zheyuanhan@163.com

0091-3286/2016/$25.00 © 2016 SPIE

Downloaded From: https://www.spiedigitallibrary.org/journals/Optical-Engineering on 9/9/2017 Terms of Use: https://spiedigitallibrary.spie.org/ss/TermsOfUse.aspx

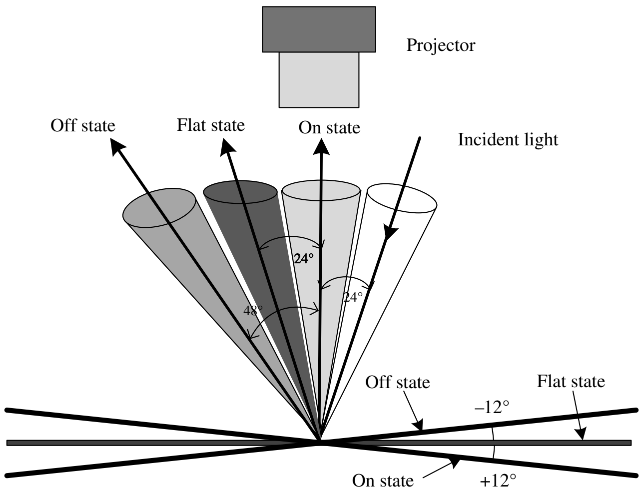

Fig. 1 The operating principle of DMD.

A and B represent the micromirrors with on states. DB is the incident waves and AC is the diffracted waves. θ_i is the incident angle, θ_r is the diffracted angle, and θ is the rotated angle. The grating constant of d is equal to d_{DMD}, where d_{DMD} is the spacing center of adjacent micromirrors.

In the long-wave IR, scalar diffraction theory is not suitable to analyze diffraction from the DMD. Instead, rigorous coupled-wave theory based on vector diffraction is required. The procedure to solve rigorous coupled-wave theory for diffraction gratings can be divided into three steps. First, the electromagnetic field in the input region is obtained from Maxwell's equations. Next, the dielectric constant of the grating region is Fourier expanded, and the resulting coupled-wave differential equations for the grating region are solved. Finally, electromagnetic boundary conditions are applied to the input region and grating region, and the diffraction efficiencies of the various diffracted orders are directly calculated.[13]

To analyze a blazed grating, the grating region is divided into many thin planar-grating slabs perpendicular to the z-axis and rigorous coupled-wave theory is applied to each slab, as shown in Fig. 3. In Fig. 3, region 1 represents the incident region, where the dielectric is air and ε_i is the relative permittivity. Region 2 represents the grating region with a relative permittivity of ε_s, and h_i is the thickness of l_j slab. In addition, the grating profile can be analyzed to an arbitrary level of accuracy provided that the individual planar gratings are sufficiently thin.[14,15]

In the previous description, the rigorous coupled-wave method treats a blazed grating of the DMD as many planar-grating slabs. The grating vector is in the plane of incidence as is the diffraction beam. The incident wave contains TE and TM polarizations. The electric field of incident TE (TM) waves is perpendicular (parallel) to the plane of incidence. In addition, the incident TM and TE waves can be analyzed independently. In this paper, for simplicity, we analyze the case of TE polarization.[16,17]

For TE polarization, the incident electric field has only a y-component. The normalized total electric field can be expressed as

$$E_{\mathrm{inc},y} = \exp[-ik_0 n_i(x \sin\theta + z\cos\theta)]. \tag{1}$$

In region 1 (the input region), the total electric field is the sum of the incident and the diffracted waves. The normalized total electric field in region 1 is expressed as

$$E_{1,y} = \exp[-ik_0 n_i(x \sin\theta + z\cos\theta)] + \sum_m R_m \exp[-i(k_{xm}x - k_{1,zm}z)], \tag{2}$$

where $i = (-1)^{1/2}$, $k_0 = 2\pi(\varepsilon_1)^{1/2}/\lambda$, k_0 is the propagation constant in region 1, λ is the incident wavelength, n_i is the refractive index, and R_m is the normalized amplitude of the m'th-order diffracted wave in region 1. Wave vectors k_{xm} and $k_{1,zm}$ are defined as

$$k_{xm} = k_0 n_i \sin\theta - \frac{2\pi m}{d}, \tag{3}$$

$$k_{1,zm} = \begin{cases} \sqrt{k_0^2 n_i^2 - k_{xm}^2} & |k_{xm}| \le k_0 n_i \\ -i\sqrt{k_{xm}^2 - k_0^2 n_i^2} & |k_{xm}| > k_0 n_i \end{cases}. \tag{4}$$

In region 1, the electric field of incident waves has only a y-component, so the magnetic field of the incident waves contains x- and z-components. The x-component of the magnetic field can be obtained from Maxwell's curl equations as

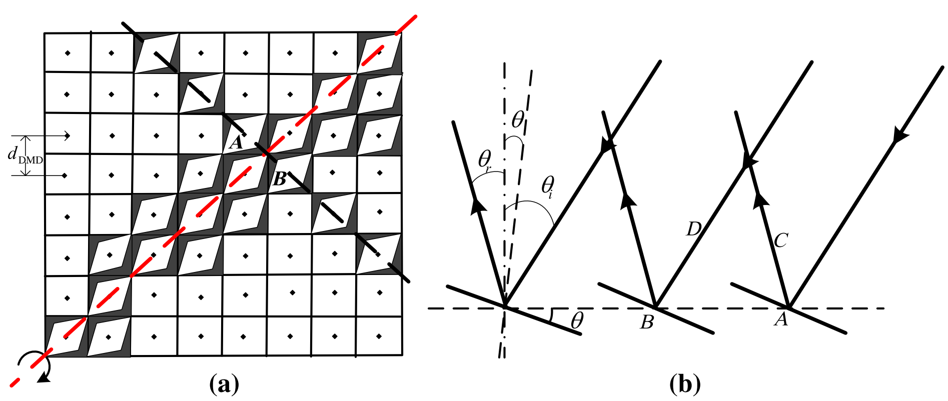

Fig. 2 Schematic view of operating DMD: (a) top view and (b) cross profile of the DMD.

Downloaded From: https://www.spiedigitallibrary.org/journals/Optical-Engineering on 9/9/2017 Terms of Use: https://spiedigitallibrary.spie.org/ss/TermsOfUse.aspx

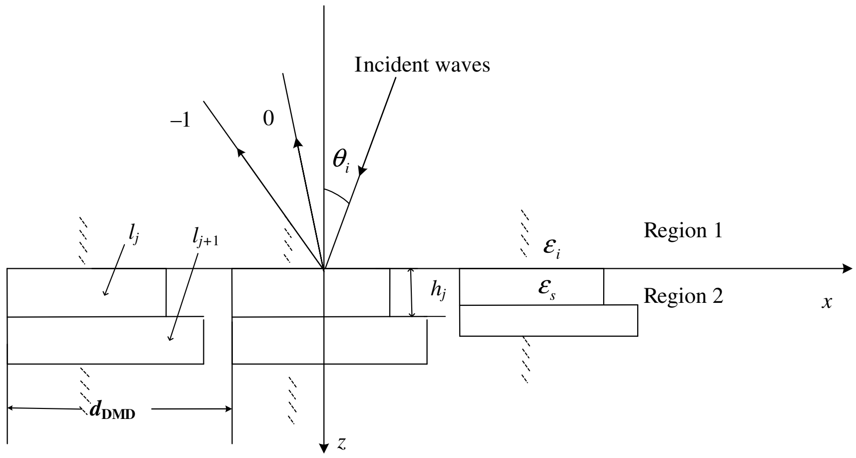

Fig. 3 Schematic depictions of layered blazed grating.

$$H_{1,x} = -\frac{k_0 n_i \cos\theta}{\omega\mu_0} \exp[-ik_0 n_i(x\sin\theta + z\cos\theta)] + \frac{1}{\omega m_0}\sum_m k_{1,zm} R_m \exp[-i(k_{xm}x - k_{1,zm})], \tag{5}$$

where ω is the angular frequency of the incident wave and μ_0 is the magnetic conductivity in a vacuum.

In region 2 (the grating region), the field can be expanded in terms of its space-harmonic components, which are phase matched to the diffracted orders in region 1. The normalized electric field and magnetic field in region 2 can be written with Fourier series

$$E_{2,y} = \sum_m S_{ym}(z)\exp(-ik_{xm}x), \tag{6}$$

$$H_{2,y} = -i\sqrt{\frac{e_0}{m_0}}\sum_m U_{xm}(z)\exp(-ik_{xm}x), \tag{7}$$

where $S_{ym}(z)$ and $U_{xm}(z)$ are the normalized electric- and magnetic-field amplitudes of the space-harmonic field, respectively. Furthermore, $E_{2,y}$ and $H_{2,y}$ satisfy Maxwell's curl equations

$$\frac{\partial E_{2,y}}{\partial z} = i\omega\mu_0 H_{2,x}, \tag{8}$$

$$\frac{\partial E_{2,y}}{\partial x} = -i\omega\mu_0 H_{2,z}, \tag{9}$$

$$\frac{\partial H_{2,x}}{\partial z} - \frac{\partial H_{2,z}}{\partial x} = i\omega\varepsilon_r\varepsilon_0 E_{2,y}, \tag{10}$$

where ε_0 is the permittivity of vacuum and ε_r is the relative permittivity of region 2.

For the l_j slab grating in region 2, the normalized electric- and magnetic-field amplitudes can be written as

$$S_{l.ym}(z) = \sum_{j=1}^{n}\omega_{l,m,j}\{a_{l,j}^{-}\exp[-q_{l,j}(z - D_l + h_j)] + a_{l,j}^{+}\exp[q_{l,j}(z - D_l)]\}, \tag{11}$$

$$U_{l.xm}(z) = \sum_{j=1}^{n} u_{l,m,j}\{-a_{l,j}^{-}\exp[-q_{l,j}(z - D_l + h_j)] + a_{l,j}^{+}\exp[q_{l,j}(z - D_l)]\}, \tag{12}$$

where h_j is the thickness of slab grating l and D_l is the total thickness of the grating, which is equal to $\sum_{j=1}^{l} h_j$.

The electromagnetic boundary conditions require that the tangential electric and magnetic fields be continuous when z is 0 or D. When z is 0, the boundary conditions lead to

$$\sum_{j=1}^{n}\omega_{j,m}[a_{1,j}^{-} + a_{1,j}^{+}\exp(-q_j h_1)] = \delta_{m0} + R_m, \tag{13}$$

$$\sum_{j=1}^{n} u_{j,m}[a_{1,j}^{-} - a_{1,j}^{+}\exp(-q_j h_1)] = i\left(n_i\cos\theta\delta_{m0} - \frac{k_{1,zm}R_m}{k_0}\right). \tag{14}$$

When z is D, the boundary conditions lead to

$$\sum_{j=1}^{n}\omega_{j,m}[a_{l,j}^{-}\exp(-q_j h_l) + a_{l,j}^{+}] = T_m, \tag{15}$$

$$\sum_{j=1}^{n} u_{j,m}[a_{l,j}^{-}\exp(-q_j D) - a_{l,j}^{+}] = \frac{i}{k_0}k_{2,zm}T_m. \tag{16}$$

For the boundary of each slab grating l_j, the boundary conditions are

$$a_{l,j-1}^{+} = a_{l,j}^{-}, a_{l,j}^{+} = a_{l,j+1}^{-}. \tag{17}$$

Equations (12)–(15) can be solved simultaneously for R_m and T_m. The diffraction efficiency of the blazing grating can be directly determined as

$$\eta_{Rm} = \mathrm{Re}\left(\frac{k_{1,zm}}{k_0 n_i\cos\theta}\right)|R_m|^2. \tag{18}$$

Downloaded From: https://www.spiedigitallibrary.org/journals/Optical-Engineering on 9/9/2017 Terms of Use: https://spiedigitallibrary.spie.org/ss/TermsOfUse.aspx

3 Diffraction Characteristics Analysis for Digital Micromirror Devices

3.1 *Diffracted Angle and Diffracted Order of the Digital Micromirror Devices*

The simulation experiment is with a DLP 700 chipset of the DMD products, which consists of 1024×768 square aluminum micromirrors. The size of a single micromirror is $13.6 \times 13.6\ \mu\text{m}^2$. As was stated in part 2, the DMD is treated as a blazed grating; the equivalent grating constant d is equal to 13.6 μm, and the blazed angle θ is 12 deg. The corresponding grating equation for the DMD can be written as[18–20]

$$d(\sin\theta_i - \sin\theta_r) = m\lambda, \tag{19}$$

where d is the grating constant, θ_i is the angle of incidence, θ_r is the angle of diffraction, and m is the diffracted order.

Figure 4 shows the optical system of a DMD-based IR scene projector, which consists of blackbody source, an illumination system, DMD, and a projector system. The projector system consists of an $F/2.6$ configuration, which means that the incident angle of the projector system must be <10.8 deg. Therefore, the diffracted angle θ_r from the DMD should be <10.8 deg when micromirrors are in the on state. At the same time, the incident angle θ_i is >10.8 deg to avoid a conflict of space between the illumination system and the projector system; actually, the incident angle θ_i is usually >20 deg. Inserting the parameters of the blazed grating into Eq. (19), diffraction angles and diffraction orders in long-wave IR are shown in Table 1. Considering the optical layout and the requirements of DMD-based scene projector, incident angle θ_i is >20 deg and diffracted angle θ_r should be <10.8 deg. From the calculation results of Table 1, it can be concluded that only first diffracted order ($m = 1$) conforms to the requirements of the scene projector system and first diffracted order is the effective order. Conclusions are drawn as follows:

1. For $\lambda = 8\ \mu$m, when θ_i is in the range of 24 to 50 deg, θ_r is <10.8 deg;
2. For $\lambda = 10\ \mu$m, when θ_i is in the range of 34 to 60 deg, θ_r is <10.8 deg;
3. For $\lambda = 12\ \mu$m, when θ_i is in the range of 44 to 60 deg, θ_r is <10.8 deg.

Generally speaking, in the long-wave IR band, when θ_i is in the range of 44 to 50 deg, θ_r is <10.8 deg.

3.2 *Diffraction Efficiency for the Digital Micromirror Devices*

The diffraction model for the DMD developed in Sec. 2.2 is based on rigorous coupled-wave theory. In this section, we use MATLAB to implement a simulation of the diffraction model and calculate the diffraction efficiency of the DMD in the long-wave IR. The MATLAB program is used for incident angles of 20 to 60 deg in 1-deg increments and with TE (TM) polarization. It simulates the diffraction energy projected with all micromirrors in the on (off) state. The results are shown in Fig. 5 and lead to the following conclusions:

1. For TE polarization, the maximum diffraction efficiency with all the micromirrors in the on (off) state is 38% (18%). The minimum diffraction efficiency with all micromirrors in the on (off) state is 13% (8%).
2. For TM polarization, the maximum diffraction efficiency with all micromirrors in the on (off) state is 85% (8%). The minimum diffraction efficiency with all micromirrors in the on (off) state is 52% (1%).

Thus, in the long-wave IR, the first-order diffraction efficiency for TM polarization is greater than that for TE polarization. In addition, for TM polarization, less diffraction light from the off state is steered into the IR scene projector.

4 Contrast Analysis for Digital Micromirror Device-Based Scene Projectors

The contrast of DMD-based scene projectors is defined as[11]

$$C = \frac{I_{\text{on}} - I_{\text{off}}}{I_{\text{on}} + I_{\text{off}}}, \tag{20}$$

where C is the contrast and $I_{\text{on}}(I_{\text{off}})$ is the diffracted intensity from the micromirrors in the on(off) state. By inserting the simulation results of Sec. 3.2 into Eq. (20), the contrast of DMD-based scene projectors for various incident angles is obtained. To facilitate the description, the contrast we list

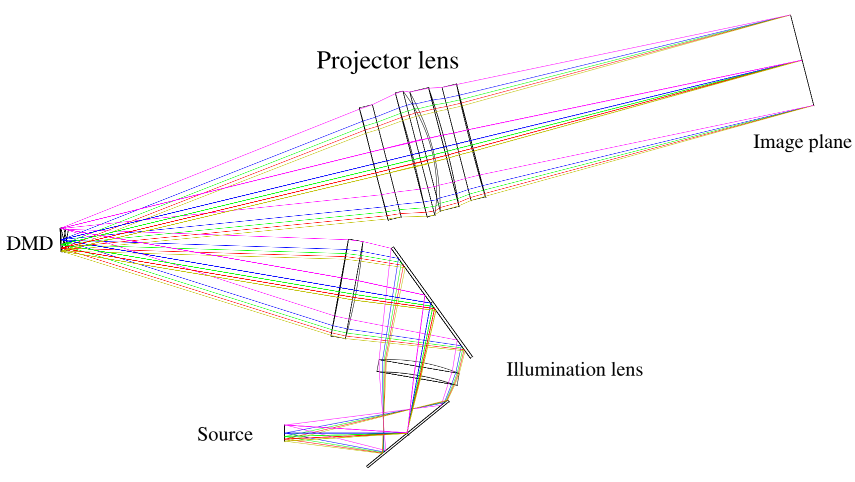

Fig. 4 Optical layout of a DMD-based IR scene projector.

Downloaded From: https://www.spiedigitallibrary.org/journals/Optical-Engineering on 9/9/2017 Terms of Use: https://spiedigitallibrary.spie.org/ss/TermsOfUse.aspx

Table 1 Diffracted angles (θ_r) of diffracted orders (m) with different wavelengths.

Incident angle (θ_i, deg)	Diffracted angles (θ_r) of different diffracted orders (m)								
	$\lambda = 8$ μm			$\lambda = 10$ μm			$\lambda = 12$ μm		
	$m = 0$ (deg)	$m = 1$ (deg)	$m = 2$ (deg)	$m = 0$ (deg)	$m = 1$ (deg)	$m = 2$ (deg)	$m = 0$ (deg)	$m = 1$ (deg)	$m = 2$
20	20	−14.3	−56.6	20	−23.1	—	20	−32.7	—
24	24	−10.5	−50.3	24	−19.2	—	24	−28.4	—
28	28	−6.8	−45.0	28	−15.4	—	28	−24.4	—
32	32	−3.3	−40.3	32	−11.8	—	32	−20.6	—
36	36	0.0	−36.1	36	−8.5	−71.8	36	−17.1	—
40	40	3.1	−32.3	40	−5.3	−63.5	40	−13.8	—
44	44	6.1	−28.8	44	−2.3	−57.5	44	−10.8	—
48	48	8.9	−25.6	48	0.5	−52.6	48	0.5	—
52	52	11.5	−22.8	44	3.1	−48.6	44	3.1	−77.7
56	56	13.9	−20.3	44	5.3	−45.2	44	5.3	−69.4
60	60	16.1	−18.1	44	7.5	−42.2	44	7.5	−64

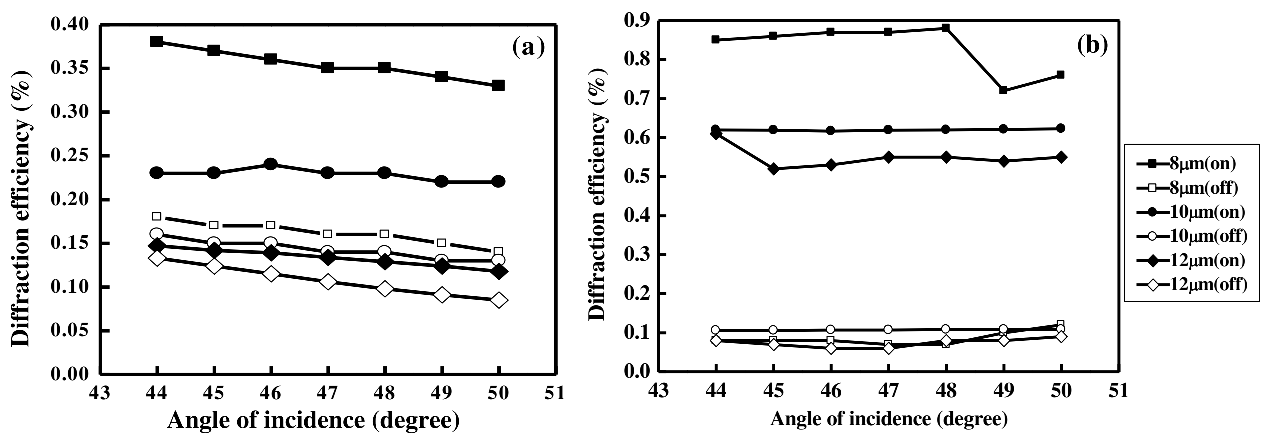

Fig. 5 First-order diffraction efficiency with θ_i (44 to 50 deg) and λ (8 to 12 μm) for (a) TE polarization and (b) TM polarization.

in Tables 2 and 3 is only for a few representative incident angles. The results lead to the following conclusions:

1. For TE polarization, the projector system delivers maximum contrast when the incident angle is 50 deg, and the contrast worsens as λ increases. In addition, for $\lambda = 8$ μm, the maximum contrast is 0.41.
2. For TM polarization, the projector system delivers maximum contrast when the incident angle is in the range of 44 to 47 deg, and the contrast improves as λ increases. In addition, for $\lambda = 10$ μm, the worst contrast is 0.7.

To summarize, the projector system obtains the maximum contrast (>0.7) in the long-wave IR band (8 to

Table 2 Contrast for DMD-based scene projector with TE polarization.

Incident angle (θ_i)		44 deg	45 deg	46 deg	47 deg	48 deg	49 deg	50 deg
Contrast (C)	$\lambda = 8$ μm	0.36	0.37	0.36	0.37	0.37	0.39	0.41
	$\lambda = 10$ μm	0.18	0.21	0.23	0.24	0.24	0.25	0.26
	$\lambda = 12$ μm	0.05	0.07	0.09	0.12	0.14	0.15	0.16

Downloaded From: https://www.spiedigitallibrary.org/journals/Optical-Engineering on 9/9/2017 Terms of Use: https://spiedigitallibrary.spie.org/ss/TermsOfUse.aspx

Table 3 Contrast for DMD-based scene projector with TM polarization.

Incident angle (θ_i)		44 deg	45 deg	46 deg	47 deg	48 deg	49 deg	50 deg
Contrast (C)	$\lambda = 8$ μm	0.83	0.83	0.83	0.85	0.85	0.76	0.73
	$\lambda = 10$ μm	0.71	0.71	0.70	0.71	0.70	0.70	0.71
	$\lambda = 12$ μm	0.77	0.76	0.80	0.82	0.75	0.72	0.71

12 μm) with an incident angle of 44 to 47 deg and with TM-polarized.

5 Conclusion

In this study, we analyze the diffraction characteristics of DMD-based scene projectors in the long-wave IR band (8 to 12 μm) using rigorous coupled-wave theory. We also simulate the diffraction model of DMD-based scene projectors using rigorous coupled-wave theory. The results lead to the conclusion that the polarization and incident angle of the incident beam are the main factors that decrease the contrast of DMD-based scene projectors in the long-wave IR. To improve the contrast of DMD-based scene projectors, we make simulations with different incident angles and different polarizations for an $F/2.6$ projector system. In the long-wave IR, the DMD-based scene projectors can get maximum contrast with an incident angle of 44 to 47 deg and with TM-polarized. This paper proposes an effective method to improve the contrast of DMD-based scene projectors in the long-wave IR.

Acknowledgments

This research was supported by the National High Technology Research and Development Program of China (Grant No. 2013AA03A116).

References

1. L. Zhang et al., "Research status and prospect of dynamic infrared scene projector," *Infrared Laser Eng.* **41**(6), 1423–1431 (2012).
2. J. Z. Zhang, "Study on the optical system of an infrared dual-band scene simulator," PhD Dissertation, Changchun Institute of Optics and Fine Mechanics and Physics, Chinese Academy of Sciences, Changchun (2013) (in Chinese).
3. L. Yang, "Study on infrared dual-band scene simulation and testing system," PhD Dissertation, Changchun Institute of Optics and Fine Mechanics and Physics, Chinese Academy of Sciences, Changchun (2012) (in Chinese).
4. J. R. Dupuis and D. J. Mansur, "Considerations for DMDs operating in the infrared," *Proc. SPIE* **8254**, 82540J (2012).
5. E. Z. Chen and P. Z. Liang, "DMD dynamic infrared scene projection technology," *Infrared Laser Eng.* **32**(4), 331–334 (2003).
6. J. R. Dupuis et al., "Two-band DMD-based infrared scene simulator," *Proc. SPIE* **7663**, 766302 (2010).
7. J. R. Dupuis et al., "High-dynamic range DMD-based IR scene projector," *Proc. SPIE* **8618**, 86180R (2013).
8. Y. Yao et al., "Design of target simulator based on DMD for infrared imaging guided system," *Laser Optoelectron. Prog.* **50**(7), 119–124 (2013).
9. Y. Q. He et al., "Diffractive characteristics of DMD and its applications in infrared scene simulation," *Laser Infrared* **43**(8), 935–938 (2013).
10. K. J. Barnard et al., "Crosstalk model of a deformable-mirror-based infrared scene projector," *Opt. Eng.* **33**(1), 140–149 (1994).
11. Y. Meuret and P. De Visschere, "Contrast-improving methods for digital micro-mirror device projectors," *Opt. Eng.* **42**(3), 840–845 (2003).
12. C. M. Chang and H. P. D. Shieh, "Design of illumination and projection optics for projectors with single digital micro-mirror devices," *Appl. Opt.* **39**(19), 3202–3208 (2000).
13. S. H. Yan, *Design of Diffractive Micro-Optics*, 1st ed., pp. 176–199, National Defense Industry Press, Beijing (2011).
14. L. F. Li and W. H. Charles, "Convergence of the coupled-wave method for metallic lamellar diffraction gratings," *J. Opt. Soc. Am. A* **10**(6), 1184–1189 (1993).
15. Y. B. Cao and H. Ai, "Calculation of vector diffraction efficiency of sub-wavelength blazed gratings," *Chin. J. Opt. Appl. Opt.* **3**(6), 679–684 (2010).
16. M. G. Moharam et al., "Rigorous coupled-wave analysis of metallic surface-relief gratings," *J. Opt. Soc. Am. A* **3**(11) 1780–1787 (1986).
17. M. G. Moharam et al., "Formulation for stable and efficient implementation of the rigorous coupled-wave analysis of binary gratings," *J. Opt. Soc. Am. A* **12**(5), 1068–1076 (1995).
18. M. H. Hutley, *Diffraction Gratings*, 2nd ed., pp. 36–38, Academic Press, New York (1982).
19. S. X. Shi, X. E. Wang, and J. S. Liu, *Physical Optics and Applied Optics*, 2nd ed., pp. 161–165, Xi Dian University Press, Xi'an (1999).
20. P. R. Joseph et al., "DMD diffraction measurements to support design of projectors for test and evaluation of multispectral and hyperspectral imaging sensors," *Proc. SPIE* **7210**, 72100D (2009).

Qing Han received his BS degree in physics from the Ocean University of China in 2012. He is a PhD student at the University of the Chinese Academy of Sciences. His current research interests include optical design and infrared optical simulation.

Jian Wang received his PhD from the University of the Chinese Academy of Sciences in 2012. He is a researcher at Changchun Institute of Optics, Fine Mechanics, and Physics, Chinese Academy of Sciences. His current research interests include optical design, optical metrology, and nonimaging optics.

Jianzhong Zhang received his PhD from the University of the Chinese Academy of Sciences in 2013. He is an assistant researcher at Changchun Institute of Optics, Fine Mechanics, and Physics, Chinese Academy of Sciences. His current research interests include infrared optical simulation, optical design, and optical metrology.

Qiang Sun is a senior researcher at Changchun Institute of Optics, Fine Mechanics, and Physics, Chinese Academy of Sciences. He has been engaged in research of infrared optics and optical precise metrology and has been in charge of many major state scientific research projects. His current research interests include infrared optical system design, optical precise alignment, and metrology.

Downloaded From: https://www.spiedigitallibrary.org/journals/Optical-Engineering on 9/9/2017 Terms of Use: https://spiedigitallibrary.spie.org/ss/TermsOfUse.aspx